Journal of Power Sources 196 (2011) 6347–6355

Contents lists available at ScienceDirect

Journal of Power Sources

journal homepage: www.elsevier.com/locate/jpowsour

Characterization of a novel, highly integrated tubular solid oxide fuel cell system using high-fidelity simulation tools

K.J. Kattke, R.J. Braun*

Division of Engineering, Colorado School of Mines, 1610 Illinois Street, Golden, CO, USA

ARTICLE INFO

Article history:
Received 31 December 2010
Received in revised form 12 March 2011
Accepted 15 March 2011
Available online 24 March 2011

Keywords:
SOFC
System analysis
Modeling
Tubular stack
Parametric study
CFD

ABSTRACT

A novel, highly integrated tubular SOFC system intended for small-scale power is characterized through a series of sensitivity analyses and parametric studies using a previously developed high-fidelity simulation tool. The high-fidelity tubular SOFC system modeling tool is utilized to simulate system-wide performance and capture the thermofluidic coupling between system components. Stack performance prediction is based on 66 anode-supported tubular cells individually evaluated with a 1-D electrochemical cell model coupled to a 3-D computational fluid dynamics model of the cell surroundings. Radiation is the dominate stack cooling mechanism accounting for 66–92% of total heat loss at the outer surface of all cells at baseline conditions. An average temperature difference of nearly 125 °C provides a large driving force for radiation heat transfer from the stack to the cylindrical enclosure surrounding the tube bundle. Consequently, cell power and voltage disparities within the stack are largely a function of the radiation view factor from an individual tube to the surrounding stack can wall. The cells which are connected in electrical series, vary in power from 7.6 to 10.8 W (with a standard deviation, σ = 1.2 W) and cell voltage varies from 0.52 to 0.73 V (with σ = 81 mV) at the simulation baseline conditions. It is observed that high cell voltage and power outputs directly correspond to tubular cells with the smallest radiation view factor to the enclosure wall, and vice versa for tubes exhibiting low performance. Results also reveal effective control variables and operating strategies along with an improved understanding of the effect that design modifications have on system performance. By decreasing the air flowrate into the system by 10%, the stack can wall temperature increases by about 6% which increases the minimum cell voltage to 0.62 V and reduces deviations in cell power and voltage by 31%. A low baseline fuel utilization is increased by decreasing the fuel flowrate and by increasing the stack current demand. Simulation results reveal fuel flow as a poor control variable because excessive tail-gas combustor temperatures limit fuel flow to below 110% of the baseline flowrate. Additionally, system efficiency becomes inversely proportional to fuel utilization over the practical fuel flow range. Stack current is found to be an effective control variable in this type of system because system efficiency becomes directly proportional to fuel utilization. Further, the integrated system acts to dampen temperature spikes when fuel utilization is altered by varying current demand. Radiation remains the dominate heat transfer mechanism within the stack even if stack surfaces are polished lowering emissivities to 0.2. Furthermore, the sensitivity studies point to an optimal system insulation thickness that balances the overall system volume and total conductive heat loss.

1. Introduction

Solid oxide fuel cells (SOFCs) are emerging as potential power sources for small-scale applications (<10 kW) including portable power, auxiliary power units (APUs), and unmanned vehicle power. In the APU market, SOFCs can achieve higher efficiencies than achieved by diesel generators with lower noise and emissions. Additionally, the high operating temperatures of SOFCs (600–1000 °C) allow on-board diesel fuel to be reformed and utilized. In portable power and unmanned vehicle applications, runtime requirements can extend from days to weeks. With increasing operating duration, the power density of SOFCs surpasses that of conventional battery technologies. While SOFCs have the potential for high power densities and efficiency, this potential is first realized with effectively packaged and thermally integrated system designs. Secondly, effective operating strategies must be identified and implemented to maximize overall SOFC performance.

Traditionally, SOFC systems are constructed by interconnecting physically separate components via fluid conduits. This approach inevitably leads to substantial void space between components which limits the maximum volumetric power density of the sys-

* Corresponding author. Tel.: +1 303 273 3055; fax: +1 303 273 3602.
E-mail addresses: kkattke@mines.edu (K.J. Kattke), rbraun@mines.edu (R.J. Braun).

0378-7753/$ – see front matter © 2011 Elsevier B.V. All rights reserved.
doi:10.1016/j.jpowsour.2011.03.030

tem. By combining process operations (such as air preheat and fuel preparation) into a single integrated unit, the potential power density is increased.

In addition to reducing the physical size of the system, the performance of the SOFC needs to be optimized in order to maximize power density. Ensuring optimal SOFC performance requires the identification of effective supervisory control variables and operating strategies. Previous parametric studies have characterized tubular cells based on the Siemens Westinghouse design [1–5]. The highly integrated stack design studied herein is dissimilar to the Siemens stack in that (i) it does not require an air-preheat tube within each cell as the oxidant flows external to (and fuel flows internal to) the tubular cells and (ii) the size of the tubes are much smaller (by a factor of 10 in length). Siemens tubular stacks consist of hundred of cells, and modeling of stack power is accomplished by aggregating the performance of a single cell without significant error [3]. The much smaller, highly integrated stack in this study consists of 66-tubular cells in which cell performance variations can lead to significant inaccuracy with the single cell approximation. High-fidelity, multi-scale simulation of SOFCs using such tools as computational fluid dynamics has largely focused on the stack alone [1–7]. Few, if any, studies in the extant literature have proceeded in scales that are inclusive of other system components. While Kattke and Braun [8] have examined the impact of component thermal interactions on system performance for planar SOFC systems, previous tubular modeling and simulation studies apply adiabatic boundaries to system components including the tail-gas combustor (TGC) and fuel reformer [1,2,5]. The integrated tubular system studied here is designed to exploit the thermal interactions between system components and the effects of which are explored through a previously developed high-fidelity system model [9]. The model evaluates each tubular cell within the stack separately and captures the thermofluidic interactions between system components.

The objectives of this steady-state analysis are to (i) identify effective supervisory control variables, (ii) reveal effective operating strategies, and (iii) understand the effect of certain system design parameters (such as the amount of insulation and surface spectral properties) on performance. While this work focuses on thermofluidic simulation of a tubular SOFC stack bundle, simulation results generated with this modeling tool could be employed as input to a separate finite element model for material stress analysis. However, the present study is not inclusive of failure-mode evaluation or prediction.

This paper begins with an overview of the previously developed high-fidelity modeling tool followed by a summary of the 'baseline' steady-state simulation results. Next, controllable system variables, including oxidant and fuel flowrates and current demand, are altered. Additionally, both surface emissivities and insulation thickness are varied to quantify the effects on system performance. The paper concludes with recommendations for the effective operation of highly integrated tubular SOFC systems.

2. SOFC system geometry

The small-scale, integrated tubular SOFC system design is shown in Fig. 1. The scope of the system study is not inclusive of pumps, blowers, and power conditioning. The focus of the work is on the integrated components within the hot zone of the packaged system. The hot zone of the system consists of a 66-tube SOFC bundle, a catalytic partial oxidation (CPOx) fuel reformer, a tail-gas comustor (TGC), a recuperator to preheat oxidant, and insulation surrounding the system. In this design, components share common walls and distinct flow piping is not required between all components. Overall system dimensions are shown in Table 1.

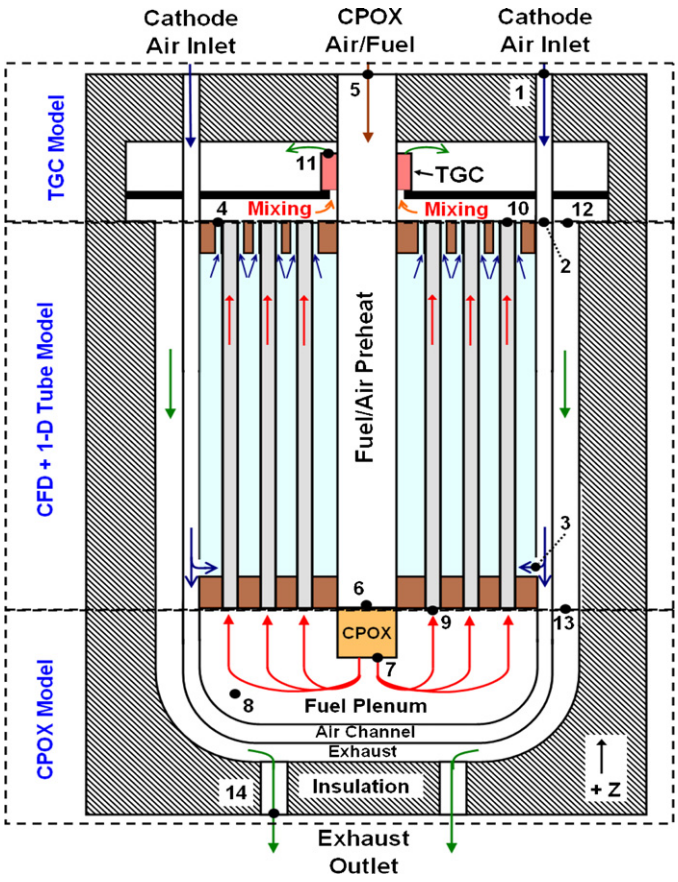

Fig. 1. Highly integrated tubular SOFC system design with statepoints. Model domains specified with dashed lines.

Table 1
System dimensions (cm).

	Height	OD	Insulation thickness
CFD domain	12.8	22.6	3.0
CPOx	6.3	22.6	2.4
TGC	5.8	21.6	3.2
System	24.9	22.3	2.9
SOFC cells	12.5 (active)	1.1	–

The system can be generalized as a centrally located tube bundle surrounded by larger cylindrical cans creating annular process flow channels. In the 66-tube bundle, anode gas flow is internal (tube-side) to and cathode gas flow is external (shell-side) to the tubular cells. The tube bundle is physically supported by an inlet tube-sheet at the anode gas entrance. Concentric circle cutouts surround each cell in the outlet tube-sheet providing an outlet for cathode gases (statepoint 4). Oxidant for the cathode enters the hot section of the packaged system through four flow tubes at the top of the system (statepoint 1), and subsequently enters an annular gas channel within the recuperator (2) where it is preheated before being radially admitted into the cathode gas region (4). A fuel/air mixture enters the system at statepoint (5) and is preheated in a centrally located flow tube prior to entering the CPOx reformer (6). Reformate leaves the CPOx unit (7) and is distributed within the fuel plenum (8) where it is assumed that the hydrogen-rich gases uniformly enter the anode gas channels (9) of the tubes. Anode and cathode exhaust gases exit the stack at statepoints (4) and (10), respectively, and mix directly above the outlet tube-sheet prior to entering the TGC. The TGC exhaust gas (11) enters the second annular gas channel of the recuperator at statepoint (12) and

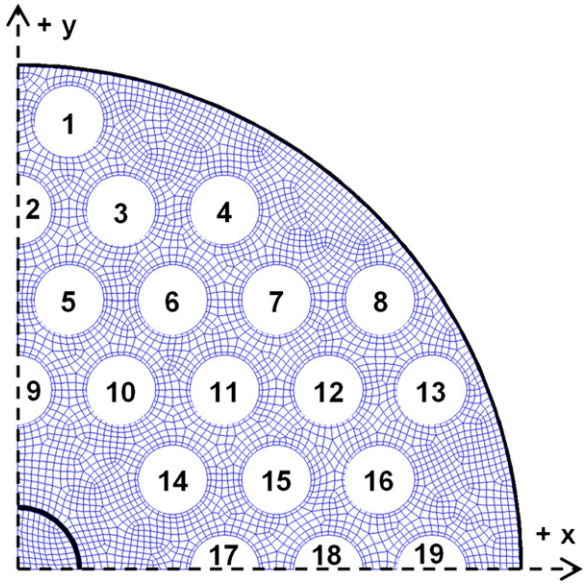

Fig. 2. 66-Tube stack arrangement. The CFD grid surrounds the domain of the tube model. Each cell is modeled independently with the tube model. Central tube is for fuel/air preheating.

finally leaves the system through flow conduits at the bottom of the system (14).

3. System modeling approach

The system is modeled with a previously developed high-fidelity tubular SOFC system model [9]. The overall system model is created by integrating four separate component level models. Fig. 1 illustrates the domains of each component model. Component models are coupled via a user-defined function (UDF) that exchanges thermodynamic states and heat transfer rates at model boundaries. A brief description of each model is described in the following sections.

3.1. 3-D CFD model

The computational fluid dynamics (CFD) software platform employed is ANSYS® FLUENT®. The domain of the CFD model includes the entire cathode and stack endplates along with the majority of the annular recuperator channels, fuel/air preheat flow, and system insulation. The outer diameter (cathode surface) of every tubular cell represents the boundary between the CFD and an electrochemical cell model. FLUENT solves the mass, energy, momentum, and species conservation equations within the computational domain of the CFD model. Radiation is modeled throughout the CFD domain utilizing a discrete ordinate radiation model assuming transparent gases. Owing to the stack symmetry (see Fig. 2), one-quarter of the system is modeled with symmetry boundary conditions applied at the *x*- and *y*-axes.

3.2. 1-D tubular cell model

A previously developed 1-D anode-supported tubular cell model is employed to model the electrochemically active cell regions [10]. The domain of the tube model includes the solid cell and the anode gas channel interior to the cell. Gas diffusion within the porous anode is modeled using the Dusty-gas model. Electrochemical performance is based on the Nernst equation with cathode and anode activation losses, concentration losses, and ohmic losses. Axial conduction is assumed to occur within the relatively thick anode structure only. All 66 cells within the bundle are modeled separately. While each cell is physically equivalent, the coupling of the CFD cathode results in a unique set of boundary conditions at the outer surface of each cell.

Table 2
Baseline simulation parameters.

Fuel/ air inlet	
Fuel type	$C_{16}H_{34}$
T (°C)	40
P (kPa)	92.65
Air inlet	
T (°C)	20
P (kPa)	84.37
Stack	
j_{avg} (A cm^{-2})	0.35
System	
CPOx: O/C	1.1
λ_{air}	2.55
Ambient	
T (°C)	20
P (kPa)	83

3.3. CPOx and TGC models

Reforming of the liquid hydrocarbon fuel feed to the system occurs within the small CPOx unit integrated within the system. Depleted anode fuel gases are oxidized in the tail-gas combustor located at the end of the tube bundle opposite to the CPOx unit. The TGC and CPOx devices including thier surrounding geometry (see Fig. 1) are modeled individually. Both models share common characteristics in that they employ quasi 1-D thermal resistance models. Lumped surface temperatures are assumed. Conduction and convection heat transfer is captured at each surface. Radiation is not explicitly modeled, but a high convective heat transfer coefficient, $h = 100\,W\,m^{-2}K^{-1}$, is utilized at all surfaces in an attempt to indirectly simulate the presence of radiation. While there is uncertainty surrounding this heat transfer coefficient, it is effectively a tuning parameter which can be varied to match model predictions to experimental data. Flow cavities are assumed perfectly mixed and include the fuel plenum, air channel, and exhaust channel in the CPOx model and the mixing and TGC exhaust regions in the TGC model. Consequently, anode flow is uniform in flowrate, temperature, pressure, and composition entering each cell of the stack.

The defining characteristics of the two models are (1) an equilibrium reformate leaves the CPOx [11,12] and (2) complete oxidation occurs in the TGC [13,14]. Additionally, flows of air and an air/fuel mixture are preheated in the TGC in which Nusselt number relationships and boiling curves are used to calculate convective heat transfer coefficients.

4. Baseline simulation

A previously performed [9] baseline simulation of the highly integrated system provides a means for comparison of the subsequent sensitivity and parametric studies. Baseline simulation parameters and performance characteristics are described in the following.

4.1. Baseline simulation parameters

The 66-cell tubular SOFC system was simulated operating on liquid hexadecane ($C_{16}H_{34}$) fuel and standard dry air. Simulation input parameters are given in Table 2. Hexadecane is a representative constituent for diesel-fueled APU applications. Cells are connected in electrical series and as a result, each cell operates at a common current. Because each cell is evaluated separately with the 1-D

Table 3
Baseline system operating conditions.

Operating conditions	
Stack power (W)	637
Stack voltage (V)	43.3
Stack current (A)	14.7
U_F	0.56
U_{Ox}	0.14
$\eta_{SOFC,\ HHV}$	25.1%
$\eta_{system,\ HHV}$	21.1%

tube model, individual cell voltages will vary from one another. The amount of stoichiometric air, λ_{air}, supplied to the system is defined as the molar flowrate of oxygen entering the system over the molar flowrate of oxygen required to completely oxide the fuel entering the system (see Eq. (1)). The O/C ratio in Table 2 represents the oxygen to carbon ratio of the gas mixture entering the CPOX reformer.

$$\lambda_{air} = \left(\frac{\dot{n}_{O_2}}{24.5 \cdot \dot{n}_{C_{16}H_{34}}} \right)_{\text{system inlet}} \quad (1)$$

4.2. Baseline simulation results

Baseline system performance metrics are displayed in Table 3 utilizing the following definitions for fuel utilization, oxidant utilization, system efficiency, and SOFC stack efficiency. U_{ox} refers to electrochemical oxidant utilization whereas λ_{air} is a system input parameter specifying the air supply rate.

$$U_F = \frac{(\dot{n}_{H_2})_{\text{stack consumed}}}{(4\dot{n}_{CH_4} + \dot{n}_{H_2} + \dot{n}_{CO})_{\text{anode inlet}}} \quad (2)$$

$$U_{ox} = \frac{(\dot{n}_{O_2})_{\text{stack consumed}}}{(\dot{n}_{O_2})_{\text{cathode inlet}}} \quad (3)$$

$$\eta_{system} = \frac{P_{DC,stack}}{(\dot{n}_{fuel} \cdot HHV_{fuel})_{\text{system inlet}}} \quad (4)$$

$$\eta_{SOFC} = \frac{P_{DC,stack}}{(\dot{n}_{fuel} \cdot HHV_{fuel})_{\text{anode inlet}}} \quad (5)$$

where $\dot{n}_i$ is the molar flowrate of species i in Eqs. (1)–(3), $P_{DC,stack}$ is the DC electrical power output of the stack, and HHV_{fuel} is the higher heating value of the hexadecane fuel. Blowers, pumps, and DC power conditioning are not included in the system simulation; therefore, DC stack power is utilized in both the SOFC and system efficiency definitions.

The baseline simulation predicts 637 W of gross output power from the stack with a system efficiency of 21.1%. The relatively low system efficiency is substantially affected by the low fuel utilization (U_F = 0.56).

Table 4 displays key temperatures throughout the system. The stack can is the cylindrical sheet metal tube that separates the cathode gases in the tube bundle from the air channel in the recuperator. An average temperature difference of nearly 125 °C develops between the relatively hot cells and the relatively cold stack can wall. The system temperatures reported in Table 4 are monitored in the subsequent analysis. The cathode inlet, anode inlet, recuperator hot side inlet, recuperator hot side outlet, and system exhaust refer to statepoints 3, 9, 12, 13, and 14 in Fig. 1, respectively.

The baseline simulation reveals radiation to be the dominate heat transfer mechanism from the cathode surface of all cells. Radiation accounts for 66–92% of total heat loss at the cell cathodes. An average 124 °C temperature difference provides a relatively large driving force for radiation heat transfer between tube surfaces and the stack can wall. Consequently, a strong relationship develops between cell power and the view factor from the cell to the stack can wall. This relationship is shown in Table 5 where cells with similar power outputs are placed in groups denoted by the dashed lines.

Cells near the outer periphery have the largest view factors to the stack can wall leading to the lowest cell temperatures and power outputs. Interior tubes achieve the highest temperatures and power outputs because outer periphery tubes act as radiation shields to the stack can. Cell power varies from 7.6 to 10.8 W (with a standard deviation, σ = 1.2 W) at outer and inner periphery tubes, respectively. As radiation to the stack can wall heavily influences cell performance, the stack performance is highly coupled to temperatures within the recuperator.

Because the stack is wired in electrical series, cell voltage varies throughout the bundle with a standard deviation of 81 mV (which is significant). In cells closest to the stack can wall, voltages are less than 0.6 V which poses a concern as the oxygen ions may begin to oxidize the nickel in the anode electrode layer. The open circuit potential for nickel oxidation at 850 °C, for instance, is estimated at 0.66 V [15,16]. As operating cell voltage is lowered beneath 0.7 V, competitive charge transfer may occur between electrochemical nickel and hydrogen oxidation. The resulting volume change within the anode microstructure upon formation of nickel oxide (NiO) increases material stresses and with enough NiO formation, eventually leads to cell rupture and/or cracking and a mechanical failure of the stack. This phenomenon is well-known among SOFC developers [17,18], yet there is currently a lack of data in the extant literature regarding establishment of an exact cell voltage range for NiO formation (e.g., see [19]). While the electrochemical rate of nickel oxidation is relatively low compared to that of hydrogen, it is likely that some anode electrode degradation will occur over extended operating periods despite low fuel utilization [19]. In addition to anode oxidation and destruction concerns, one must be aware of the lower voltage limit into the DC converter. Ultimately, the electrical side of the system and any associated impact on the inverter is outside the scope of this study as the primary focus is related to the thermofluidic interactions within the system boundary under analysis. The voltage and power density relationship to current density for the cells is shown in Fig. 3. Results are extracted from single cell simulations utilizing the baseline anode conditions, average baseline cathode composition, and fixing the cell temperature.

5. Sensitivity analysis and parametric study

The novel, highly integrated system is characterized through a series of sensitivity analyses and parametric studies. First, system operating parameters are varied including oxidant and fuel flowrates and current demand. These operating parameters are physically manipulated by varying the pump, blower speeds, and the power electronics. Therefore, the response of the system to these parameters provides insight into how one might better control the system. Next, cathode emissivity, stack can emissivity, and insulation thickness design parameters are varied to gauge their

Table 4
Baseline system temperatures (°C).

Stack (Avg)	Stack can (Avg)	Cathode inlet	Anode inlet	Recup. hot side-inlet	Recup. hot side-outlet	System exhaust
745	621	668	816	868	657	683

Table 5
Baseline stack performance (grouped by similar power outputs).

Grouping	Cell #	Power (W)	View factor to stack can[a]	Normalized position[b]	T_{avg} (°C)	Voltage (V)
1	13	7.61	0.463	0.90	694.4	0.52
	8	7.66	0.463	0.90	695.4	0.52
	1	7.68	0.463	0.90	695.6	0.52
2	19	8.25	0.400	0.83	707.0	0.56
	4	8.37	0.400	0.83	709.4	0.57
3	16	9.44	0.208	0.74	734.6	0.64
	7	9.55	0.208	0.74	737.5	0.65
	3	9.59	0.208	0.74	738.4	0.65
4	12	10.03	0.143	0.72	751.4	0.68
	2	10.10	0.143	0.72	753.6	0.69
5	18	10.34	0.096	0.62	761.6	0.70
	6	10.42	0.096	0.62	764.3	0.71
6	15	10.68	0.021	0.55	774.9	0.73
	11	10.71	0.021	0.55	776.3	0.73
	5	10.75	0.020	0.55	778.0	0.73
	17	10.77	0.012	0.41	778.5	0.73
	10	10.80	0.011	0.41	780.0	0.73
	14	10.79	0.006	0.36	779.4	0.73
	9	10.81	0.006	0.36	780.2	0.73

[a] Calculated in ANSYS FLUENT.
[b] The radial distance from the center of the stack to the center of the cell is normalized by the radius of the stack can wall.

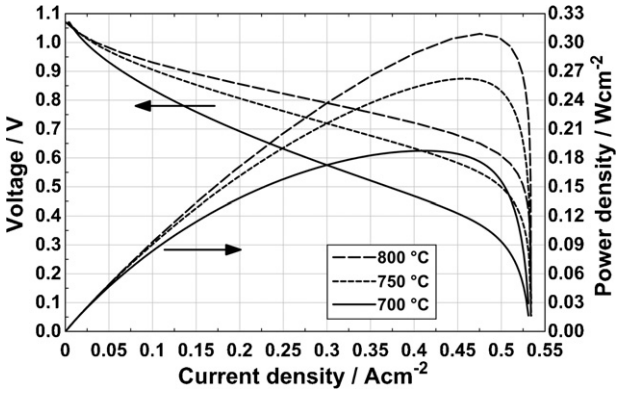

Fig. 3. Cell voltage and power density curves at various cell temperatures.

influence on system performance. In all studies, a single operating or design parameter is modified with all other parameters held fixed during any given simulation.

5.1. Air flowrate

Performance characteristics of the system are explored with respect to air flowrate. Results of varying the air flowrate into the system by ±10% from the baseline (2.41×10^{-3} kg s^{-1}) are shown in Table 6.

Table 6
Parameter sensitivity to air flowrate.

Variable	% Change from baseline	
Air flowrate	−10	+10
Parameters		
$T_{stack\ (avg)}$	3.7	−3.1
$T_{stack\ can\ wall\ (avg)}$	5.9	−4.9
$T_{cathode\ inlet}$	6.0	−5.1
$T_{anode\ inlet}$	3.8	−3.1
$T_{recup.\ hot\ side\text{-}inlet}$	4.5	−3.6
$T_{recup.\ hot\ side\text{-}outlet}$	5.5	−4.4
$T_{exhaust}$	5.2	−4.2
Stack power	8.7	−9.7
η_{sys}	8.7	−9.8

A decreased air flowrate results in higher temperatures throughout the system. The stack can wall temperature increases by 5.9% because of higher exhaust temperatures and an increased thermal capacitance ratio of exhaust to air in the recuperator. As the stack can wall temperature increases, the large temperature difference between the stack and its surroundings is reduced. The average cell temperature increases 3.7% resulting in an 8.7% increase in stack power and system efficiency. The effect of air flowrate on individual cell powers is shown in Table 7. Outer periphery tubes (groupings 1 and 2) with the largest view factor to the stack can wall experience the greatest increase in cell power where as inner periphery tubes (groups 6 and 7) have the smallest increase in cell power. Therefore, a reduction in air flow promotes a more uniform distribution of cell power among the tubes. The standard deviation of cell voltages is reduced to 56 mV (31% decrease from the baseline), and the lowest cell voltage is increased to 0.62 V. Thus, the concern of Ni oxidation

Table 7
Cell power sensitivity to air flowrate.

Variable		% Change from baseline	
Air flowrate		−10	+10
Grouping	**Cell #**		
1	13	19.0	−18.9
	8	18.8	−18.8
	1	18.8	−19.0
2	19	15.7	−16.2
	4	15.2	−16.1
3	16	9.9	−10.9
	7	9.4	−10.7
	3	9.2	−10.3
4	12	7.1	−8.1
	2	6.8	−8.0
5	18	6.1	−7.3
	6	5.8	−7.2
6	15	4.7	−5.9
	11	4.6	−5.9
	5	4.5	−5.8
	17	4.5	−5.8
	10	4.4	−5.7
	14	4.4	−5.8
	9	4.4	−5.8

Table 8
System sensitivity to fuel flowrate.

Variable	% Change from baseline	
Fuel flowrate	−10	+10
Parameters		
$T_{stack\ (avg)}$	−3.9	4.6
$T_{stack\ can\ wall\ (avg)}$	−6.8	7.6
$T_{cathode\ inlet}$	−6.9	7.4
$T_{anode\ inlet}$	−5.4	5.3
$T_{recup.\ hot\ side\text{-}inlet}$	−9.4	9.8
$T_{recup.\ hot\ side\text{-}outlet}$	−7.5	8.0
$T_{exhaust}$	−6.9	7.2
Stack power	−13.7	11.1
η_{sys}	−4.1	1.0
U_F	11.0	−9.0

Table 9
Parameter sensitivity to cell current.

Variable	% Change from baseline	
Cell current	−10	+10
Parameters		
$T_{stack\ (avg)}$	−0.2	0.3
$T_{stack\ can\ wall\ (avg)}$	1.5	−1.3
$T_{cathode\ inlet}$	1.4	−1.3
$T_{anode\ inlet}$	0.5	−0.5
$T_{recup.\ hot\ side\text{-}inlet}$	3.9	−3.8
$T_{eecup.\ hot\ side\text{-}outlet}$	2.0	−1.9
$T_{exhaust}$	1.6	−1.5
Stack power	−6.0	5.6
η_{sys}	−6.0	5.6

from low cell voltage operation is also reduced. Inverse relations apply when air flow is increased.

5.2. Fuel flowrate

A low baseline system efficiency (η_{sys} = 21%) is primarily a result of a relatively low fuel utilization (U_F = 56%). Fuel utilization is manipulated by varying the fuel flowrate into the system by ±10% from the baseline (4.02×10^{-4} kg s^{-1}). The effects on system performance are presented in Table 8. In this analysis, a constant O/C ratio of 1.1 is maintained. With stack current held constant, fuel utilization is inversely proportional to the fuel flowrate.

While a 10% reduction in fuel flowrate increases fuel utilization to 62.6%, it is accompanied by a 13.7% decrease in stack power that results in a 4.1% lowering of system efficiency. The reduction in stack power is a consequence of lower cell temperatures due to an increased ΔT to the stack can wall. The stack can wall temperature drops significantly (by nearly 7%) because both the thermal capacitance and temperature of the hot exhaust gases entering the recuperator decrease as the fuel flowrate are reduced.

Opposite trends are seen when the fuel flowrate is increased. Surprisingly, an increased fuel flowrate results in an *increased* system efficiency even though fuel utilization is lowered to 51.3%. The increase in energy input into the system is outweighed by the power increase from the stack. This inverse relationship between system efficiency and fuel utilization when the latter is controlled by fuel flowrate is explored further in the following parametric study.

The effect of fuel flowrate on performance is examined in the range of 90–140% of the baseline input condition. The resulting stack power and system efficiency curves over this range are shown in Fig. 4. The maximum efficiency, 21.5%, occurs at approximately 108% of the baseline fuel flowrate. Efficiency remains near the maximum as fuel flow is varied ±10% from the 108% optimal. Moving further from the optimal flowrate, efficiency begins to dramatically decrease dropping below 19% (a 12% decrease from maximum) at 140% fuel flow.

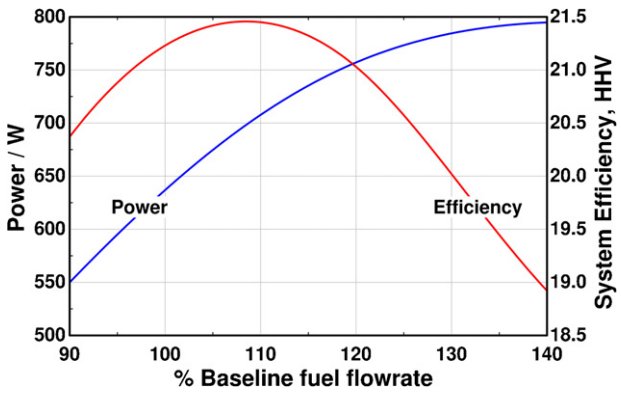

Fig. 4. Parametric study varying fuel flowrate.

Stack power continuously increases over the range of fuel flow studied, but the rate of increasing power declines as fuel flow increases. The temperatures in/around the CPOx and TGC must be monitored with any changes to fuel flowrate. The temperature of reformate leaving the CPOx reformer ranges from 1218 to 1270 °C at fuel flows of 100–140% of the baseline, respectively. Both cathode and anode exhaust temperatures increase with increased fuel flow causing TGC exhaust temperatures to increase significantly. TGC exhaust increases from about 1000 to 1420 °C at fuel flows of 100–140% of the baseline, respectively. Prolonged operation at these high gas temperatures could cause catalyst sintering. Thus, fuel flow should not be increased past 110% of the baseline which corresponds to a 1101 °C TGC exhaust temperature. System efficiency remains inversely proportional to fuel utilization over the majority of the practical fuel flow range (up to 108% of the baseline).

5.3. Cell current

Another method to increase fuel utilization is to increase the current demand from the stack. As cells are wired in electrical series, the stack current and fuel utilization are directly proportional. The following analysis reveals whether altering fuel flowrate or cell current is the most effective strategy to control fuel utilization. Table 9 shows the sensitivity of the system to a ±10% change in operating current from the baseline (14.7 A or 0.35 A cm^{-2}).

Stack power and system efficiency are both directly proportional and the most sensitive parameters to operating current. Consequently, system efficiency is directly proportional to fuel utilization when the latter is controlled with cell current. Fuel utilization ranges from 50.7 to 62.0% at −10% and +10% cell current, respectively.

System temperatures are relatively insensitive to changes in cell current with the stack temperature showing relatively no dependence. This is a result of a temperature regulating effect created by the integrated system design. At lower currents, the magnitude of cell irreversibilites is lowered which tends to decrease cell temperatures, but more unspent fuel entering the TGC causes the stack can wall temperature to increase which tends to increase cell temperatures. At higher current demands, cell irreversibilities increase which tend to increase cell temperatures, but less thermal energy entering the recuperator lowers the stack can wall temperature which tends to lower cell temperatures. A self-regulating system allows for simplified operating strategies as current can be varied without the need to simultaneously vary other system parameters in order to maintain system temperatures and thereby, power.

To identify the stack current that maximizes stack power, current is increased to 150% of the baseline with results presented in Fig. 5. In this simulation, reactant gas flowrates were held at

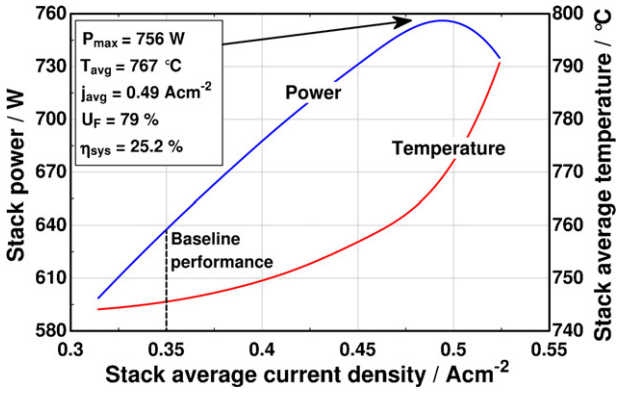

Fig. 5. Parametric study performed on cell current.

their baseline values. As Fig. 5 shows, the stack power curve has the same relationship to current density as seen at the cell level. Stack power increases with current density until a peak is reached after which stack power decreases as concentration overpotentials begin to substantially limit cell voltage.

Fig. 5 shows a maximum stack power of 756 W occurring at a current density of 0.49 A cm^{-2}. Stack power reaches a maximum at the same current density as a single cell operating at the stack average temperature, 767 °C. The stack temperature increases with current density due to increasing cell irreversibilities, but the stack temperature remains relatively insensitive to current density as the temperature only increases by about 6% over the current range explored. Fuel utilization is linearly dependent to stack current ranging from 51 to 85% at the lower and upper limits of current density, respectively. The system efficiency is directly proportional to fuel utilization for all current densities below peak power.

5.4. Fuel utilization control

It is often desirable to operate SOFCs at higher fuel utilizations (>70%) in order to reduce hot spots in the TGC, lower fuel storage requirements, and increase system efficiency. While fuel utilization is not directly controllable, varying the fuel flowrate and/or cell current allows the fuel utilization to be altered. Simulation results highlight current demand as the most effective method to indirectly control fuel utilization. When varying the stack current, the integrated system design acts to dampen any temperature spikes. Secondly, fuel utilization is directly proportional to system efficiency until peak stack power. Finally, stack power is related to current density in the same manner as cell power. Since power density curves for cells are well known, calculating a current demand set point near the peak power density is relatively straightforward if the stack temperature is known.

Varying fuel flowrate is not an effective method of fuel utilization control. TGC temperatures spikes limit the fuel flowrate to no more than 110% of the baseline. Varying the fuel flowrate within this range, the system efficiency and fuel utilization are inversely proportional. Lastly, any increase in fuel flow will require larger fuel storage tanks lowering the power density of the system.

5.5. Surface emissivity

Heat transfer at the cathode surface of all cells is dominated by radiation (66–92% of surface heat transfer). Therefore, the dependence of stack performance on surface emissivities within the stack is explored. The emissivity of YSZ-LSM cathodes is dependent on proprietary manufacturing techniques and measured reference values are lacking in the literature. Thus, the effect of the baseline $\varepsilon_{cathode}$ = 0.8, which is consistent with prior models in the extant literature [20,4], is explored. An existing SOFC model [21] utilized a cell emissivity of 0.33 which illustrates the wide range and uncertainty in cell emissivity values. The emissivity at the stack can wall is also explored because its value can be altered with various surface finishes. The baseline wall emissivity of 0.9 is representative of an oxidized INCONEL® 600 alloy [22], and using polished stainless steel could reduce the emissivity near 0.30 [23].

Table 10
Parameter sensitivity to cathode and stack can emissivity.

	Stack cathode		Stack can wall	
Variable	% Change from baseline			
Emissivity	−10	+10	−10	+10
Parameters				
$T_{stack\ (avg)}$	0.1	0.0	0.1	−0.1
$T_{stack\ can\ wall\ (avg)}$	−0.1	0.1	−0.3	0.2
$T_{cathode\ inlet}$	−0.1	0.1	−0.3	0.2
$T_{anode\ inlet}$	−0.2	0.0	−0.1	0.0
$T_{recup.\ hot\ side\text{-}inlet}$	0.0	0.0	0.2	−0.2
$T_{recup.\ hot\ side\text{-}Outlet}$	−0.1	0.0	−0.2	0.1
$T_{exhaust}$	−0.1	0.0	−0.1	0.1
Stack power	0.2	−0.2	0.3	−0.3
η_{sys}	0.3	−0.1	0.3	−0.1

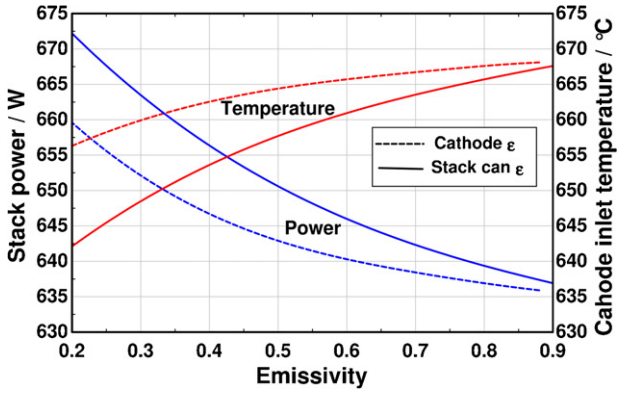

Fig. 6. Parametric study varying emissivity at cathode external surface of the cell.

A sensitivity analysis, presented in Table 10, reveals little system dependence on cathode and stack can emissivity values near the baselines of 0.8 and 0.9, respectively. With the non-linearities in radiation heat transfer, both surface emissivities are further explored as the linear relationship shown in Table 10 is not likely to hold true for a larger range of emissivities.

Stack power along with the cathode inlet temperature are shown in Fig. 6 as a function of cathode and stack can emissivities. A non-linear relationship to both surface emissivities is observed for both the stack power and cathode inlet temperature. Overall, sensitivity to cathode emissivity remains relatively low. Stack power and the cathode inlet temperature change by 3.7% and 1.8%, respectively, corresponding to a decrease from 0.88 to 0.2 in the cathode emissivity. Simulation results suggest a more precise cathode emissivity is not required.

Similarly, the sensitivity to the stack can emissivity is low. Stack power and the cathode inlet temperature change by 5.9% and 4.0%, respectively, corresponding to a decrease from 0.99 to 0.2 in the stack can emissivity. An economic analysis could determine if the benefit of increased stack power outweighs the additional cost of improving the surface finish and thereby, lowering the stack can emissivity.

5.6. Insulation thickness

Insulation is wrapped around the system to hinder the transport of thermal energy out of the system. While adding insulation

Table 11
Parameter sensitivity to insulation thickness.

Variable	% Change from baseline	
Insulation thickness	−10	+10
Parameters		
$T_{stack\ (avg)}$	−0.2	0.1
$T_{stack\ can\ wall\ (avg)}$	−0.3	0.2
$T_{cathode\ inlet}$	−0.3	0.2
$T_{anode\ inlet}$	−0.2	0.2
$T_{recup.\ hot\ side\text{-}inlet}$	0.0	−0.1
$T_{recup.\ hot\ side\text{-}outlet}$	−0.3	0.2
$T_{exhaust}$	−0.3	0.3
Stack power	−0.4	0.4
η_{sys}	−0.4	0.4

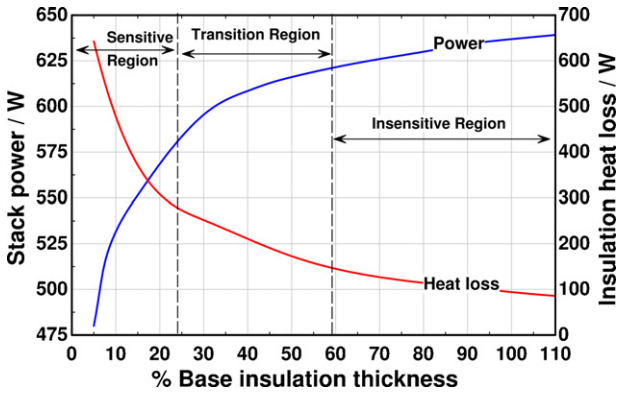

Fig. 7. Parametric study varying insulation thickness around system.

lowers heat loss to the surroundings, it comes at the expense of a larger system and increased material costs. The baseline insulation thickness (2.9 cm) allowed 94 W to be conducted to the system surroundings. Baseline insulation is sufficiently thick as 94 W is only 3.1% of energy entering the system. The parametric analysis shown in Table 11 reveals all system statepoints and performance metrics are insensitive to insulation thickness near the baseline. This result indicates the baseline insulation is over-sized and warrants subsequent simulations with decreasing insulation thickness.

Fig. 7 depicts the relationship between stack power and insulation heat loss as a function of insulation thickness. Stack power and heat loss remain relatively unchanged as insulation is decreased to 60% of the baseline. A transition region occurs where stack power and heat loss become sensitive to insulation thicknesses ranging from 25 to 60% of the baseline. Insulation no longer represents a significant thermal resistance at thicknesses below 25% of the baseline because stack power decreases significantly. Operating at the junction of the transition and insensitive regions would result in the thinnest insulation without a significant decrease in stack power.

6. Conclusion

A novel, highly integrated tubular SOFC system has been characterized with a series of sensitivity analyses and parametric studies. Controllable system variables were first varied including the air flowrate, fuel flowrate, and stack current demand. The effects of system design modification were also investigated by varying surface emissivities around the stack and the insulation thickness surrounding the system. All results are based on a previously developed high-fidelity tubular SOFC system model. The model captures the high level of thermofluidic coupling within the integrated system. While the model would benefit from experimental validation, the following general operating characteristics and conclusions can be made:

1. Radiation is the dominate heat transfer mode within the stack and cell power variations are coupled to radiation view factors to the walls surrounding the stack. Disparities in tube power can be reduced by raising the temperature of the walls surrounding the bundle.
2. Small-scale tubular stacks do not rely on convective heat transfer alone for stack cooling. This characterstic tends to reduce the air flow requirements of the system. Reducing air flow also effectively increases the wall temperatures surrounding the stack which produces more uniform cell powers and voltages.
3. Fuel flowrate is an ineffective control variable because of its limited range due to temperature spikes in the TGC. Additionally, the system efficiency is inversely proportional to fuel utilization over the applicable fuel flow range.
4. Stack current is an effective control variable because system efficiency is directly proportional to fuel utilization for current below the maximum power density. Secondly, the integrated system acts to dampen temperature spikes when the cell current is varied.
5. Radiation remains the dominate heat transfer mechanism from the stack even when emissivity values around the stack are substantially lowered. Radiation will always be an effective stack cooling method for small-scale tubular stacks.

This paper has focused on a novel, highly integrated tubular SOFC system design, but the high-fidelity modeling tool employed is also applicable to larger SOFC systems of varying architectures. Simulation results can aid SOFC developers in developing effective system designs and identifying attractive operating strategies. Furthermore, it should be noted that the modeling approaches taken herein are also applicable to technologies analogous to fuel cells, such as tubular water-gas shift membrane reactors.

Acknowledgments

The authors would like to thank Dr. Robert Kee for his helpful suggestions and for facilitating the collaborative effort with ANSYS-FLUENT and Dr. Graham Goldin at ANSYS-FLUENT. Funding for this work was provided by the U.S. Department of Energy, Office of Energy Efficiency & Renewable Energy (EERE) under contract number DE-FG36-08GO88100.

References

[1] F. Calise, G. Ferruzzi, L. Vanoli, Parametric exergy analysis of a tubular solid oxide fuel cell (SOFC) stack through finite-volume model, Appl. Energy 86 (2009) 2401–2410.
[2] S. Campanari, Thermodynamic model and parametric analysis of a tubular SOFC module, J. Power Sources 92 (2001) 26–34.
[3] D. Sanchez, R. Chacartegui, A. Munoz, T. Sanchez, Thermal and electrochemical model of internal reforming solid oxide fuel cells with tubular geometry, J. Power Sources 160 (2006) 1074–1087.
[4] J. Jia, A. Abudula, L. Wei, R. Jiang, S. Shen, A mathematical model of a tubular solid oxide fuel cell with specified combustion zone, J. Power Sources 171 (2007) 696–705.
[5] W. Jiang, R. Fang, J.A. Khan, R.A. Dougal, Parameter setting and analysis of a dynamic tubular SOFC model, J. Power Sources 162 (2006) 316–326.
[6] N. Autissier, D. Larrain, J. Van herle, D. Favrat, CFD simulation tool for solid oxide fuel cells, J. Power Sources 131 (2004) 313–319.
[7] S.F. Lee, C.W. Hong, Multi-scale design simulation of a novel intermediate temperature micro solid oxide fuel cell stack system, Int. J. Hydrogen Energy 35 (2010) 1330–1338.
[8] K.J. Kattke, R.J. Braun, Implementing thermal management modeling into SOFC system level design, ASME, J. Fuel Cell Sci. Technol. (2011), doi:10.1115/1.4002233.
[9] K.J. Kattke, R.J. Braun, A.M. Colclasure, G. Goldin, High-fidelity stack and system modeling for tubular SOFC system design and thermal management, J. Power Sources 196 (2011) 3790–3802.
[10] A.M. Colclasure, B.M. Sanandaji, T.L. Vincent, R.J. Kee, Modeling and control of tubular solid-oxide fuel cell systems. I: physical models and linear model reduction, J. Power Sources 196 (2011) 196–207.

[11] J. Krummenacher, K. West, L. Schmidt, Catalytic partial oxidation of higher hydrocarbons at millisecond contact times: decane, hexadecane, and diesel fuel, J. Catalysis 215 (2003) 332–343.
[12] K. Hohn, T. DuBois, Simulation of a fuel reforming system based on catalytic partial oxidation, J. Power Sources 183 (2008) 295–302.
[13] M. Sorrentino, C. Pianese, Control oriented modeling of solid oxide fuel cell auxiliary power unit for transportation applications, J. Fuel Cell Sci. Technol. 6 (2009).
[14] N. Lu, Q. Li, X. Sun, M.A. Khaleel, The modeling of a standalone solid-oxide fuel cell auxiliary power unit, J. Power Sources 161 (2006) 938–948.
[15] D. Sarantaridis, R.A. Rudkin, A. Atkinson, Oxidation failure modes of anode-supported solid oxide fuel cells, J. Power Sources 180 (2008) 704–710.
[16] P. Nehter, A high fuel utilizing solid oxide fuel cell cycle with regard to the formation of nickel oxide and power density, J. Power Sources 164 (2007) 252–259.
[17] A. Wood, M. Pastula, D. Waldbillig, D.G. Ivey, Initial testing of solutions to redox problems with anode-supported SOFC, J. Electrochem. Soc. 153 (10) (2006) A1929–A1934.
[18] J. Van herle, D. Larrain, N. Autissier, Z. Wuillemin, M. Molinelli, D. Favrat, Modeling and experimental validation of solid oxide fuel cell materials and stacks, J. Eur. Ceram. Soc. 25 (2005) 2627–2632.
[19] R.W. Sidwell, W.G. Coors, Thermodynamic limits of electrical efficiency in hydrocarbon fueled SOFC using internal reforming, SOFC-IX, Quebec, Canada, ECS Meeting Abstracts 501 (2006) 1240.
[20] F. Calise, M.D. d'Accadia, G. Restuccia, Simulation of a tubular solid oxide fuel cell through finite volume analysis: effects of the radiatve heat transfer and exergy analysis, Int. J. Hydrogen Energy 32 (2007) 4575–4590.
[21] X. Xue, J. Tang, N. Sammes, Y. Du, Dynamic modeling of single tubular SOFC combining heat/mass transfer and electrochemical reaction effect, J. Power Sources 142 (2005) 211–222.
[22] Special Metals, INCONEL 600 Data Sheet, product data sheet, Table 3, p. 2, September, 2008.
[23] F. Incropera, D. DeWitt, T. Bergman, F. Lavine, Fundamentals of Heat and Mass Transfer, 6th ed., Wiley, New York, 2007.